Original scientific paper

Screen-printed carbon electrode/natural silica-ceria nanocomposite for electrochemical aptasensor application

Salma Nur Zakiyyah[1], Diana Rakhmawaty Eddy[1], M. Lutfi Firdaus[2], Toto Subroto[3] and Yeni Wahyuni Hartati[1,✉]

[1]Department of Chemistry, Faculty of Mathematics and Sciences, Universitas Padjadjaran, Jl. Raya Bandung-Sumedang km. 21 Jatinangor, Sumedang 45363, Indonesia
[2]Graduate School of Science Education, bengkulu University, Jl. W.R. Supratman Kandang Limun, Bengkulu 38371, Indonesia
[3]Bionformatics and Biomolecular Research Center, Universitas Padjadjaran, Jl. Singaperbangsa 2, Bandung 40132, Indonesia

Corresponding author: ✉*yeni.w.hartati@unpad.ac.id*

Abstract

A nanocomposite of natural silica and ceria was synthesized to modify a screen-printed carbon electrode (SPCE) to develop an aptasensor to detect epithelial sodium channel (ENaC) protein in urine as a biomarker of hypertension. The method steps were the synthesis of natural silica-ceria nanocomposite using the hydrothermal method, obtaining of natural silica nanoparticles from the extraction of alkaline silica sand and ceria nanoparticles from cerium nitrate, modification of SPCE/natural silica-ceria, immobilization of aptamer through streptavidin-biotin, and detection of ENaC protein concentration. Box-Behnken's design was employed to determine the optimal con-ditions of aptamer concentration (0.5 µg mL^{-1}), streptavidin incubation time (30 min), and aptamer incubation time (1 hour), respectively. Differential pulse voltammetry (DPV) characterization of the developed electrochemical aptasensor revealed that the $[Fe(CN)_6]^{3-/4-}$ redox peak current increased from 3.190 to 9.073 µA, with detection and quantification limits of 0.113 and 0.343 ng mL^{-1}, respectively. The method is proven as a simple and rapid method to monitor ENaC levels in urine samples.

Keywords

Silica-ceria; synthesis composite, aptamer; ENaC protein; hypertension biomarker; voltammetry

Introduction

In the development of electrochemical-based biosensor methods, electrode modification is the most important step to immobilize bioreceptors onto the electrode surface [1]. In addition

of improving biosensor performance, the basic functions of nanoparticles can be mainly classified as: 1) immobilization of biomolecules; 2) catalysis of electrochemical reactions; 3) enhancement of electron transfer; 4) labeling biomolecules and 5) acting as the reactant [2]. Many types of nanomaterials have been reported to modify electrode surfaces, for example, a screen-printed carbon (SPCE) immunosensor was modified with AuNP [3-8], and SPCE aptasensor was modified with ceria [3,9,10]. Silica-based nanocomposites have been widely developed as electrode modifiers, such as silica-Au nanocomposite for the detection of the enzyme glucose oxidase [11], c-creative protein [12], and arsenic detection [5]. Silica-modified SPCE for sensors has already been reported [5,13,14] . It is worth noting that SPCE is an electrode that combines a carbon working electrode, Ag/AgCl reference electrode, and carbon counter electrode in one compact and easy-to-use design [15].

Silica nanoparticles can be made into composites with metal nanoparticles [16]. Silica nanoparticles used for dopamine detection in biosensors demonstrate excellent performance and low detection limits [17]. Silica composites are used in electrochemical sensors because they have a very high specific surface area [5], while biologically modified silica composites in mono or multilayer configurations are commonly applied in electroanalysis, especially in the field of biosensors [18]. Silica-ceria composite is an interesting material because silica can improve the thermal stability and texture of ceria. Typically, silica-ceria composites are synthesized by the hydrothermal method [19] with silica obtained from various sources or precursors. Natural sand is a commonly use source of silica which is mixed with oxides and other minerals and therefore, a separation is needed to obtain pure silica by the alkaline fusion method [20]. Up to now, SPCE electrode modified with natural silica-ceria composite has never been carried out, and only synthetic silica was applied in biosensors to detect some inorganic compounds [21,22]. One of the uses of natural silica produced from natural sand in this study [20] is to stabilize ceria nanoparticles.

Ceria nanoparticles are transition metal oxide (CeO_2) elements that have good potential in the development of biosensors with high electron mobility due to high oxygen storage capacity in its structure, redox transition ability, enhanced electron transfer, biocompatibility, and high conductivity. All these properties improve sensitivity, selectivity, stability, and long-term maintenance of biosensor bioactivity [23]. When $Ce(NO_3)_3 \cdot 6H_2O$ is added to the silica dispersion, the positively charged Ce^{3+} ions are attracted to the surrounding silica through electrostatic interactions, and precipitate on the surface of the silica in a weakly alkaline environment [24]. Ceria from the silica-ceria composite strongly interacts with $-NH_2$ groups to bind streptavidin and thionine for the matrix metalloproteinase-2 biosensor, and can form a bridge bond with the carboxyl functional group of the antibody even without the addition of other agents [3]. The amphipathic protein structure can non-specifically bind to the silica surface due to the curvature of the silica and the molecular weight, protein affinity constants, as well as the adsorption process. Adsorption as a non-covalent electrostatic interaction model, with the layer by layer (LbL-ESA, or LbL) electrostatic assembly method is used in bioconjugation with silica [25]. By comparing the effect of the size of the material on the electrode, Damiati *et al*. [26] showed that it has a direct impact on the electrochemical response and sensitivity of the biosensor. It is known that smaller sized electrodes exhibit higher sensitivity, attributed to the better structural material properties due to the presence of the nearest neighbor.

Based on previous research, a biosensor can detect hypertension with the ENaC protein biomarker [27]. Hypertension occurs when an individual experiences increase in blood pressure

above normal and is associated with increased morbidity and mortality [28]. The epithelial sodium channel (ENaC) is a major regulator of salt and water reabsorption in many epithelial tissues, while abnormalities of ENaC function are directly associated with hypertension [29]. The ENaC controls the rate limiting step of sodium reabsorption in epithelial cells and is located on the apical membrane of cells in the distal nephron which is responsible for controlling Na^+ reabsorption. ENaC protein in urine is a biomarker of hypertension as ENaC expression promotes Na^+ retention, leading to an increase in blood pressure [30,31].

Typically, ENaC protein is detected by enzyme-linked immunosorbent assay (ELISA) [4,32], but this method is time consuming and expensive [27]. Immunosensors can detect low levels of ENaC [3,31] since using antibodies as bioreceptors is highly selective and sensitive [33]. However, antibody based methods are relatively expensive for commercial purposes and therefore alternative methods have been developed, such as the determination of ENaC protein levels through its interaction with aptamers [34]. Aptamers are single stranded RNA or DNA synthetic oligonucleotides selected through *in vitro* method known as Systematic evolution of ligands by exponential enrichment (SELEX) which can bind to its target with high affinity and specificity due to its three-dimensional structure. The advantages of aptamers over antibodies are high stability, easily synthesis and modification, low immunogenicity, and possibility of recognition a wide variety of molecules [5]. Thus aptasensors have high affinity, lower costs, and are easier to modify [35]. The use of streptavidin to bind to biotinylated aptamers has already been reported [8,36] . The biotinylated aptamer in this study was used from a previous study [37]. This paper reports the development of an aptasensor using a modified silica-ceria SPCE to detect ENaC protein as a biomarker of hypertension.

Experimental

The materials used were biotinylated aptamer (biotin 5'- CGG TGA GGG TCG GGT CCA GTA GGC CTA CTG TTG AGT AGT GGG CTC C -3') (Abcam), ENaC protein, bovine serum albumin (BSA), potassium ferricyanide $K_3[Fe(CN)_6]$ (Sigma Aldrich), streptavidin (Promega), phosphate buffer saline (PBS) pH 7.4 (VWR), potassium chloride (KCl) (Merck), sodium hydroxide (NaOH) (Merck), absolute ethanol (Merck), methanol (Merck), cerium nitrate $(Ce(NO_3)_3.6H_2O)$ (Merck), sample urine (non-hypertention) and double distilled water (PT. Ikapharmindo Putramas).

Screen-printed carbon electrode (SPCE) (DWG No. 9601626, GSI Technologies, USA) consisting of the carbon working electrode (WE), carbon counter electrode (CE), and reference Ag/AgCl electrode (RE), (Zimmer and Peacock), connected to a computer using software PSTrace 5.8. Fourier transform infra-red (FT-IR) spectrometer (Thermo Scientific), *scanning electron microscopy* (SEM) (Hitachi TM3000), particle size analyzer (PSA) (Horiba SZ-100), and UV-Vis spectrophotometer (Thermo Scientific G10S UV-Vis).

Preparation of silica-ceria nanocomposites

Ceria nanoparticles were synthesized by first dissolving 2 g of cerium nitrate hexahydrate $(Ce(NO_3)_3 \cdot 6H_2O)$ in 50 mL double distilled water before the dropwise addition of 25 mL (0.1 M) sodium hydroxide (NaOH) solution with constant stirring for 30 minutes at room temperature. The pale yellowish white precipitate formed within 1 hour, and was collected by centrifugation at 8000 rpm for 20 min. The pellets were washed by double distilled water several times, dried at 70 °C for 2 hours, and cooled to room temperature before calcining at 240 °C overnight to obtain the nanoparticle ceria powder that was characterized by UV-Vis spectroscopy, FT-IR, and PSA [38].

Silica was obtained from in house synthesis as previously described [39]. The ceria-silica composite was prepared by mixing 4.5 mL of distilled water and 14.5 mL of absolute ethyl alcohol and stirring sonochemically for 15 minutes before addition of 0.018 g of ground silica. The solution was stirred sonochemically for 3 minutes and 0.1031 g of solid ceria was added and mixed for 45 minutes. Immediately after mixing, 10 mL of double distilled water was added and stirred continuously for 20 minutes. The solution was centrifuged for 10 minutes at 6000 rpm and the silica-ceria composite was then dried at 110°C for 2 hours and calcined at 500 °C for 5 hours before redissolving in 50 mL methanol. The composites were made in various concentrations (0.007, 0.01, and 0.03 mM). The ceria-silica composite was characterized by UV-Vis spectroscopy, FTIR, and SEM [40].

Characterization of silica-ceria nanocomposite

In this work, particle size analyzer (PSA, Horiba SZ-100) was used to characterize the particle sizes, scanning electron microscopy (SEM, Hitachi TM3000) to characterize the surface morphology of electrodes, and UV-Vis spectrometer (Thermo Scientific G10S UV-Vis) to analyze the UV block properties of the samples. The stability of the surface functional groups was examined by FTIR (Thermo Scientific), while differential pulse voltammetry (DPV, Zimmer and Peacock) was used for electrochemical measurements.

Preparation of SPCE

SPCE electrodes were washed twice to remove impurities physically adsorbed on the electrode surface with double distilled water, then dried at room temperature and characterized using SEM and DPV in 10 mM $K_3[Fe(CN)_6]$ solution in 0.1 M KCl as the supporting electrolyte [21].

Modification of SPCE with silica-ceria nanocomposite

The composite solution was dropped onto the surface of the SPCE and allowed to dry before rinsing with double distilled water and characterized using SEM-EDS and DPV performed as for bare SPCE [11].

Immobilization of streptavidin on SPCE/silica-ceria

Ten microliters of 50 µg mL^{-1} streptavidin solution was dropped onto the surface of the SPCE/silica-ceria and incubated in the refrigerator. The obtained SPCE/silica-ceria/STV electrodes were rinsed and characterized using SEM-EDS and DPV as described above [11].

Immobilization of biotinylated aptamer on SPCE/silica-ceria/STV

Ten microliters of 0.5 µg mL^{-1} aptamer-biotin solution was added to the dry SPCE/silica-ceria/STV, and then measured by DPV as in previous stages [11].

Determination of aptasensor response to ENaC protein

Fifteen microliters *of* 1 % BSA was added to the electrode for 20 minutes, then rinsed by double distilled water before 15 µL of ENaC solution was dropped onto the electrode and incubated for 20 minutes. Then, DPV was performed in conditions described in previous sections. The schematic of this aptasensor preparation and testing is shown in Figure 1.
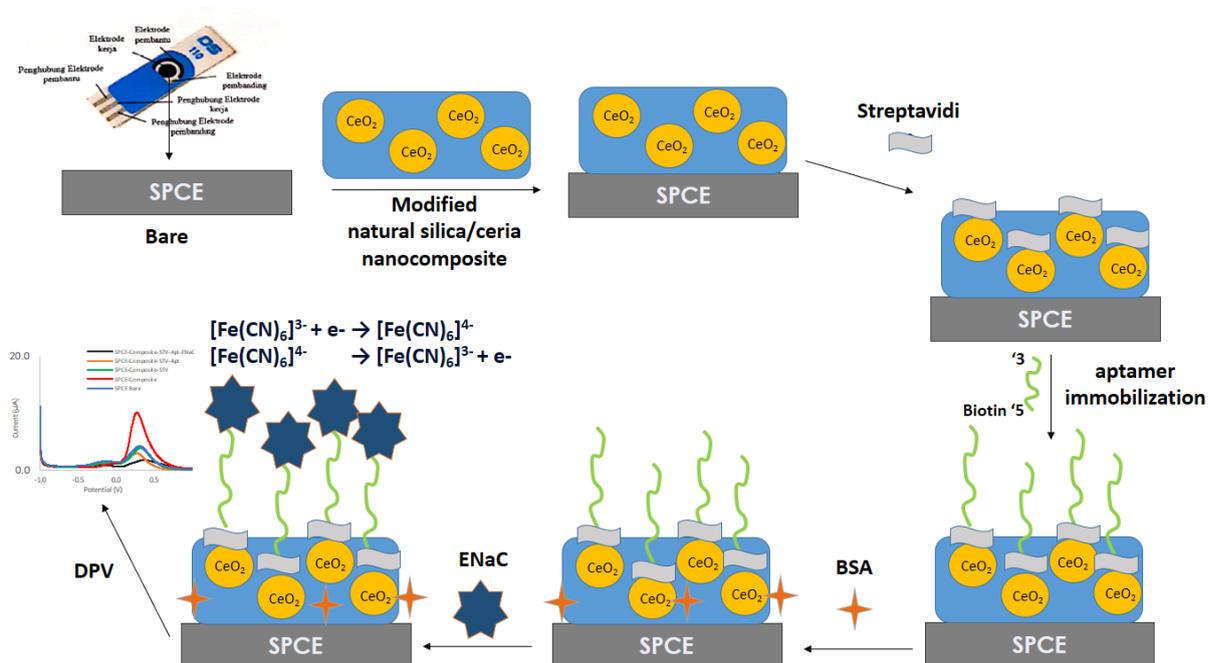
Figure 1. *Preparation and testing of electrochemical aptasensor using a nanocomposite-streptavidin-aptamer to detect ENaC protein*

Optimization of parameters using the Box-Behnken method

The parameters used were variations in the concentration of the ENaC aptamer (X_1), the incubation time of the SPCE-nanocomposite (X_2), and the incubation time of the SPCE-nanocomposite-aptamer (X_3). The factor is designed through 3 different levels, namely the lowest (-1), medium (0), and highest (+1) level, as shown in Table 1.

Table 1. *Factors and levels of optimization analysis of experimental conditions*

Factor	Level		
	-1	0	+1
ENaC aptamer concentration (X_1), mg mL^{-1}	0.5	1	1.5
Streptavidin incubation time (X_2), min	30	60	90
ENaC aptamer incubation time (X_3), h	1	2	16

Calibration curve, detection limit, and quantification limit

Various concentrations of ENaC solutions (0.047, 0.094, 0.187, 0.375, 0.75, 1.5 and 3.0 ng mL^{-1}) were measured by the electrochemical aptasensor with differential pulse voltammetry (DPV) method, in 0.1 M KCl containing $[Fe(CN)_6]^{4-/3-}$ redox system. The potential range of -1.0 to +1.0 V and a scan rate of 0.008 V/s using the optimal conditions determined from the Box-Behnken method. A linear curve of the difference between average peak current values (ΔI) *vs.* the concentration for each measurement was evaluated to determine limits of detection (LOD) and quantification (LOQ), precision, and recovery values.

Determination of ENaC recovery in urine samples

Samples were prepared by the standard addition method [41,42], *i.e.* 20 µL urine sample was spiked with 2 µL of various concentrations of ENaC (1, 2, and 3 ng mL^{-1}), and 2 µL of phosphate buffer saline (PBS) was used as a control. The electrochemical response of aptasensor was measured by DPV using a redox system of 10 mM K$_3$[Fe(CN)$_6$] solution in 0.1 M KCl, in the potential range of -1.0 to +1.0 V at a rate of scan 0.008 V/s.

Results and discussion

Characterization of ceria NPs, silica-ceria composite, and SPCE

Characterization of the precipitated synthesized ceria, silica-ceria composite, and modified SPCE is shown in Figures 2-4.

Figure 2a shows the UV-Vis spectrophotometry results of ceria particles, showing a peak at 308 nm which is within the normal range of 250-400 nm [43]. This peak is produced by the transition of electrons from the 2p O level to the 4f Ce level and by the 4f-5d electronic transition in Ce^{3+} [44]. Based on Figure 2b, the silica nanoparticles showed a peak at 300 nm with an average particle size of 99.7 nm. The ceria-silica nanocomposite in Figure 2c showed absorption peak at maximum wavelength of 337 nm, with a small peak at 231 nm. The maximum wavelength peak range for the ceria-silica composite is 250–400 nm [24] as reported by Dalmis *et al*. [45], and Vaja *et al*. [46], where a small shoulder observed is around 200–300 nm. The UV-Vis absorbance of most of the ceria comes from the charge transfer transition from O 2p to Ce 4f, and the spectrum shows two overlapping absorption peaks caused by the indirect and direct transitions. Usually, the absorption edge energy is calculated assuming direct and indirect transitions [46].
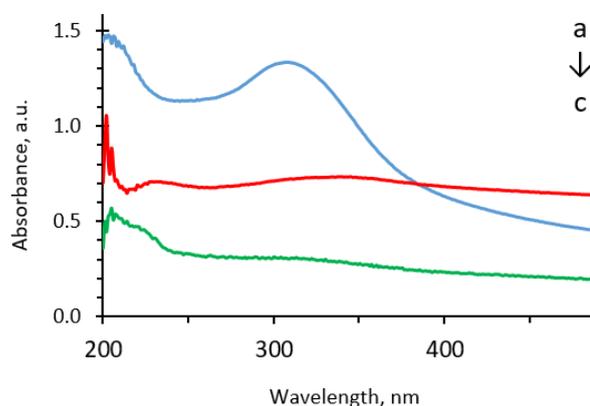
Figure 2. *UV-Vis characterization of (a) ceria with a maximum absorption wavelength at 308 nm, (b) ceria-silica nanocomposite with a maximum absorption wavelength at 337 nm and a small peak at 231 nm, (c) silica nanoparticles with a maximum absorption wavelength at 300 nm*

Figure 3a of the particle size analyzer (PSA) characterization shows that the ceria particles were 251.6 nm in size, classifying them as microparticles as they were >100 nm. Figure 3b shows that the silica nanoparticles were 99.7 nm, *i.e.* nanoparticles. In this study, a composite modified electrode with composites that are materials consisting of two or more materials that have different properties with their constituent properties remaining in the resulting material [47].

The electrodes were modified with composites silica-ceria in 1:2 mole ratio as in a previous study [24]. Silica particles have a smooth surface and are negatively charged in neutral or basic dispersions. When $Ce(NO_3)_3 \cdot 6H_2O$ is added to the silica dispersion, the positively charged Ce^{3+} ions are attracted to the vicinity of SiO_2 through electrostatic interactions and precipitate on the surface of SiO_2 in a weakly alkaline environment.

Figure 4a shows the FTIR characterization of the silica-ceria nanocomposite, with peaks at 3440.9 cm^{-1} indicating OH stretching, 549.35 cm^{-1} (Ce-O), 1621.51 cm^{-1} (OH bonding, 1095.3 cm^{-1} (Si-O-Si), and 491.28 cm^{-1} (Si-O). Figure 4b shows the peak at a frequency of 549.35 cm^{-1} confirming Ce-O bond [44,48] . Figure 4c shows a peak at 1097.973 cm^{-1} indicating Si-O-Si bonds and 421.24 cm^{-1} Si-O bonds [39].
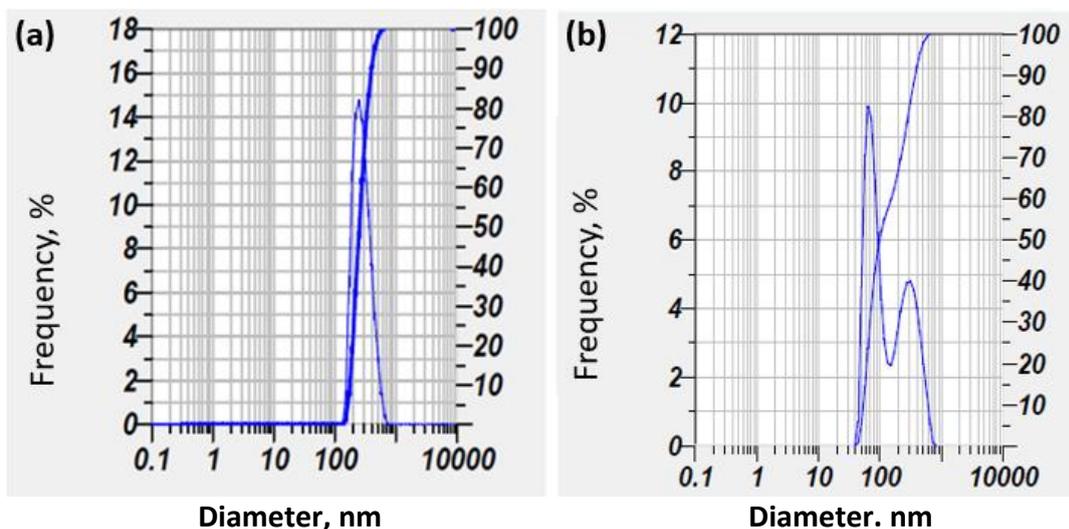
Figure 3. *PSA characterization of (a) ceria particles with a size of 251.6 nm and (b) silica nanoparticles with a size of 99.7 nm*
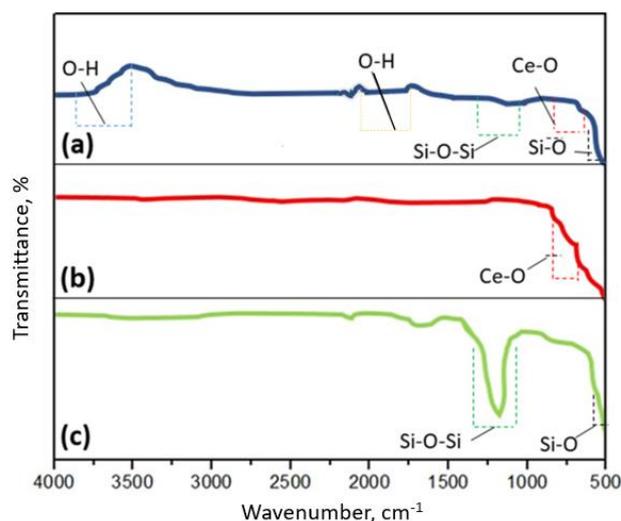
Figure 4. *FTIR spectra of (a) ceria-silica nanocomposite, (b) ceria particles, (c) silica nanoparticles*

Characterization and modification of SPCE

Figure 5 shows the surface morphology of the SPCE modified by silica-cerium and biomolecules, taken with the scanning electron microscope (SEM). Figure 5a shows the morphology of the bare SPCE surface. In Figure 5b, the surface of SPCE after modification by the silica-ceria nanocomposite looks different in morphology, suggesting that the composite is attached to the SPCE surface. After immobilization of streptavidin biomolecules, Figure 5c shows that SPCE surface looks more homogeneous and denser than before. More homogeneous and denser surface morphology shown in Figure 5d for SPCE-nanocomposite after addition of the aptamer also confirms that the electrode surface has been changed. Some of chemical elements of SCPE-ceria-silica nanocomposite and that modified by biomolecules, determined by the EDS test shown in Figure 5e and f, are listed in Table 2. According to Table 2, four elements are contained in the composite-modified SPCE, namely carbon (a component of the SPCE electrode), oxygen, silicon, and cerium (components of composite), indicating thus the successful modification of the SPCE electrode by ceria-silica composite. Also, Table 2 shows that SPCE-nanocomposite modified by streptavidin biomolecules contains carbon, oxygen, silicon, and cerium as well as nitrogen contained in the streptavidin protein, indicating the successful modification of the SPCE-nanocomposite electrode by streptavidin biomolecule.
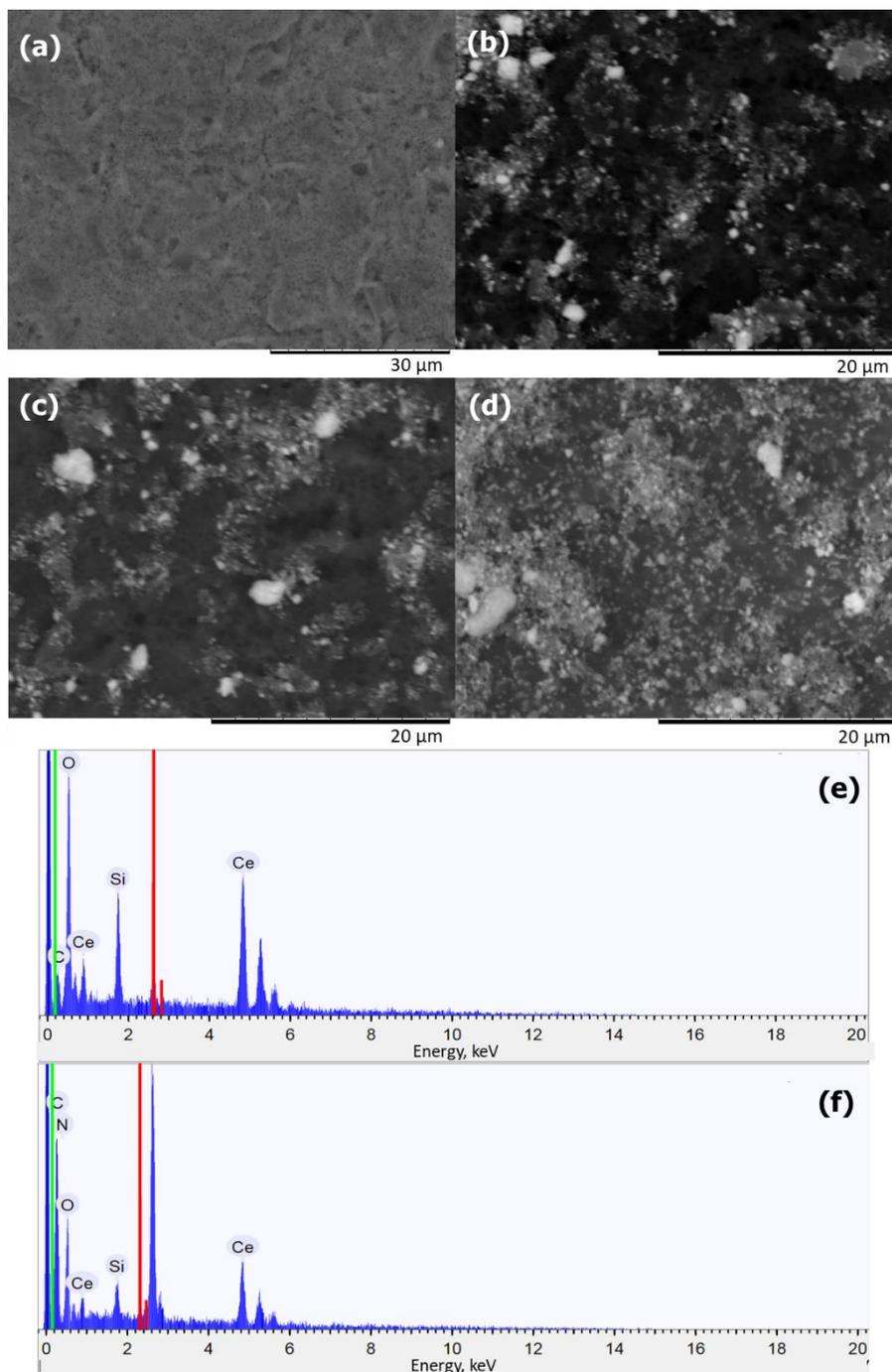
Figure 5. *SEM characterization of (a) bare SPCE; (b) SPCE-nanocomposite; (c) SPCE-nanocomposite-streptavidin; (d) SPCE-nanocomposite-streptavidin-aptamer, and EDS of (e) SPCE-nanocomposite surface; (f) SPCE-nanocomposite-streptavidin surface*

Table 2. *EDS characterization the modified SPCE*

Element	SPCE-nanocomposite	SPCE-nanocomposite-streptavidin
	Content, wt. %	
Carbon	8.699	37.601
Oxygen	29.260	24.130
Silicon	7.024	2.275
Cerium	55.017	32.621
Nitrogen	-	3.372

The modification of the SPCE with various concentrations of nanocomposite (0.007, 0.01 and 0.03 mM) was characterized by differential pulse voltammetry (DPV) in 0.1M KCl containing 10 mM $K_3[Fe(CN)_6]$, in the potential range of -1.0 to +1.0 V at a scan rate of 0.008 V/s. Figure 6a shows that the highest $[Fe(CN)_6]^{3-/4-}$ redox peak current was obtained with 0.01 mM concentration, while at higher concentration of composite (0.03 mM), a decrease in the redox peak current occurs (Table 3). Silica-ceria composite material is semi-conductor [16,49] that can increase electron transfer at certain concentrations and conditions. In this experiment, the data obtained at the concentration of 0.01 mM has an optimum current of ferri-ferrocyanide reaction, while at higher concentration, the insulator properties increased. Anyhow, Figure 6b shows that modification of the electrode is needed to increase the sensitivity to the required biosensor sensing. Figure 6b presents the characterization of bare SPCE electrode and SPCE electrodes modified with composites and biomolecules, showing firstly an increase in current due to the presence of composite at SPCE, and then a decrease in the current after the addition of biomolecules (Table 3). The electrode is modified with biomolecules which function to make a specific bond in the biosensor analysis. Biomolecule s are large and not conductive, thereby inhibiting electron transfer which results in a decrease in the redox peak current of $K_3[Fe(CN)_6]$. As shown in Figure 6b and Table 3, a modification of the electrode is ultimately needed to increase the sensitivity to the biomarker.
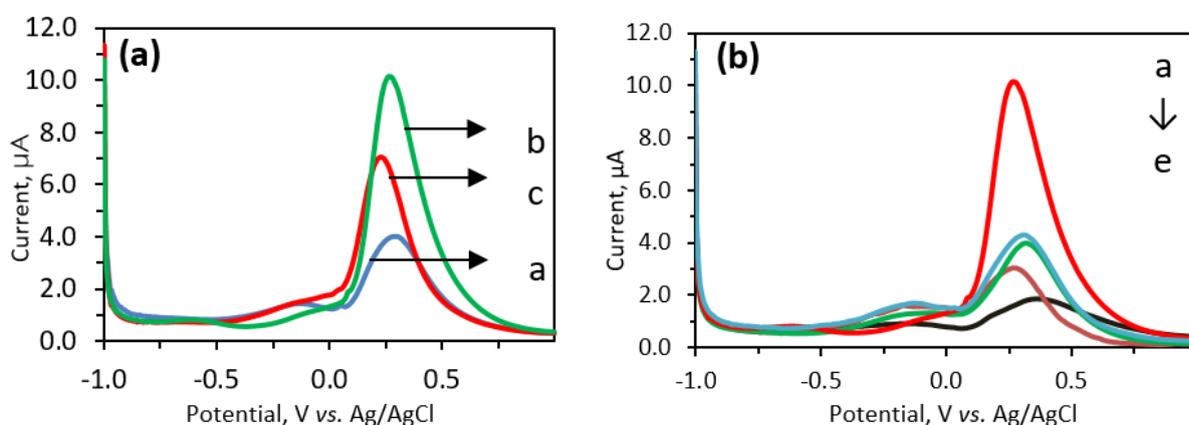
Figure 6. *DPVs of 10 mM $K_3[Fe(CN)_6]$ in 0.1M KCl at: (a) SPCE aptasensor for different composite concentrations a → c (0.007, 0.01, 0.03) mM and (b) a → g (SPCE-composite; SPCE bare; SPCE-composite-STV; SPCE-composite-STV-Apt; SPCE-composite-STV-Apt-ENaC)*

The use of biomolecules in biosensors, especially electrochemical, is growing as they allow rapid and sensitive detection. In this study, a streptavidin biomolecules was added to the electrode surface to bind specifically to the ENaC aptamer [37] with a biotin tag. The interaction between the aptamer (Apt) and the ENaC protein was analyzed using the Biovia Discovery Studio Visualizer, showing that the compound has eleven hydrogen bonds, one hydrophobic interaction, and six electrostatic interactions with four unfavorable interactions or electrostatic repulsion [37]. The interactions that occur are hydrogen bonds, van der Waals forces, and are hydrophobic. The streptavidin-biotin interaction also binds like an antibody to an antigen *via* non-covalent interaction between the protein and ligand [2].

Streptavidin has four identical subunits, each of which can bind biotin with high affinity and specificity, and non-covalent bond interactions occur when biotin binds to tryptophan in the subunit. The non-covalent bond formed between biotin and streptavidin has a higher binding

affinity than most antigen and antibody bonds and is of similar strength to a covalent bond. Two amino acids play a role in avidin-biotin interactions, namely tryptophan and lysine [2].

Table 3. DPV characterization the modified SPCE

Electrode modified	Peak current, µA
SPCE bare	3.190
SPCE-Composite 0.007 mM	3.063
SPCE-Composite 0.01 mM	9.673
SPCE-Composite 0.03 mM	6.544
SPCE-Composite-STV	3.115
SPCE-Composite-STV-Apt	2.043
SPCE-Composite-STV-Apt-ENaC	1.229

Streptavidin on the surface of the SPCE-nanocomposite will interact with ceria and protein adsorption can occur due to electrostatic interactions, hydrophobic interactions, and specific chemical interactions between proteins and nanoparticles, and is influenced by pH and concentration [50]. If the pH of the acid buffer creates a positive zeta potential due to the increased concentration of H^+ ions, the ceria is dispersed with PBS pH 7.4, thus increasing adsorption of protein on ceria in the composite.

Ceria in the silica-ceria composite strongly interacts with $-NH_2$ groups to bind streptavidin and thionine for the matrix metalloproteinase 2-biosensor, forming a bridge bond with the carboxyl functional groups of the antibody, even without the addition of other agents [3]. The amphipathic protein structure can bind to the silica surface non-specifically, due to the curvature of the silica and the molecular weight, protein affinity constants as well as the adsorption process. Adsorption as a non-covalent electrostatic interaction model, with the layer by layer (LbL-ESA, or LbL) electrostatic assembly method, was used in bioconjugation with silica [25].

Characterization and performance of aptasensor

The aptamer used in this study was a modeled ENaC specific ssDNA aptamer designed using simRNA (69 nt). The charge on the aptamer is negative because it has a phosphate group that interacts with positive amino acid residues (arginine, histidine, lysine). The interaction of aptamer with ENaC protein is electrostatic, with good structural complementarity of the aptamer ENaC and hydrogen bonding. The interaction between the aptamer and ENaC was measured by DPV based on electron transfer from the $[Fe(CN)_6]^{3-/4-}$ redox system. Figure 6b shows redox peak currents for streptavidin, interaction of the streptavidin-aptamer and interaction of the aptamer ENaC on the electrode surface. A significant decrease in the redox peak current value is seen when the ENaC protein is attached specifically to the aptamer (Table 3).

Experimental optimization according to Box-Behnken method

The aptamer concentration (X_1), streptavidin incubation time (X_2), and ENaC aptamer incubation time (X_3) were evaluated *via* Box-Behnken experiment design. The experimental data resulted in the following regression equation:

$$Y = -1.379 + 0.597X_1 + 0.0688X_2 + 0.484X_3 + 0.004X_1^2 - 0.000463X22 -$$
$$- 0.02091X_3^2 - 0.00927X_1X_2 - 0.0459 X_1X_3 - 0.000667X_2X_3 \qquad (1)$$

Based on equation (1), a factor with a negative value affects decreasing the response, while for a factor with a positive value it affects increasing the response in the experiment. ANOVA

analysis of the Box-Behnken experiment revealed the P-values of each factor as $X_1 = 0.0499$; $X_2 = 0.5358$; $X_3 = 0.0001$. The P-value of 0.05 indicates that the factor is significant. In addition, the P-value of the less of fit (LOF) obtained in this experiment is 0.2047 (>0.05) so it can be concluded that the resulting linear model is appropriate. LOF indicates a deviation or inaccuracy to the linear model so that the tests carried out aim to detect whether the linear model is appropriate. The Behnken Box data revealed optimum conditions for ENaC aptamer concentration of 0.5 µg mL^{-1}, 30 min incubation of the streptavidin protein, and 1-hour incubation of the ENaC aptamer.

Calibration curve, detection limit, and quantification limit

Figure 7a displays the characterization results of the ENaC aptasensor, showing that the current decreased with increasing ENaC concentration, since more biomolecules are blocked on the electrode surface, thereby reducing the current. The ENaC protein is a large biomolecule and is not electroactive, so at higher ENaC concentration, higher is inhibition of the $[Fe(CN)_6]^{3-/4-}$ electron transfer process.
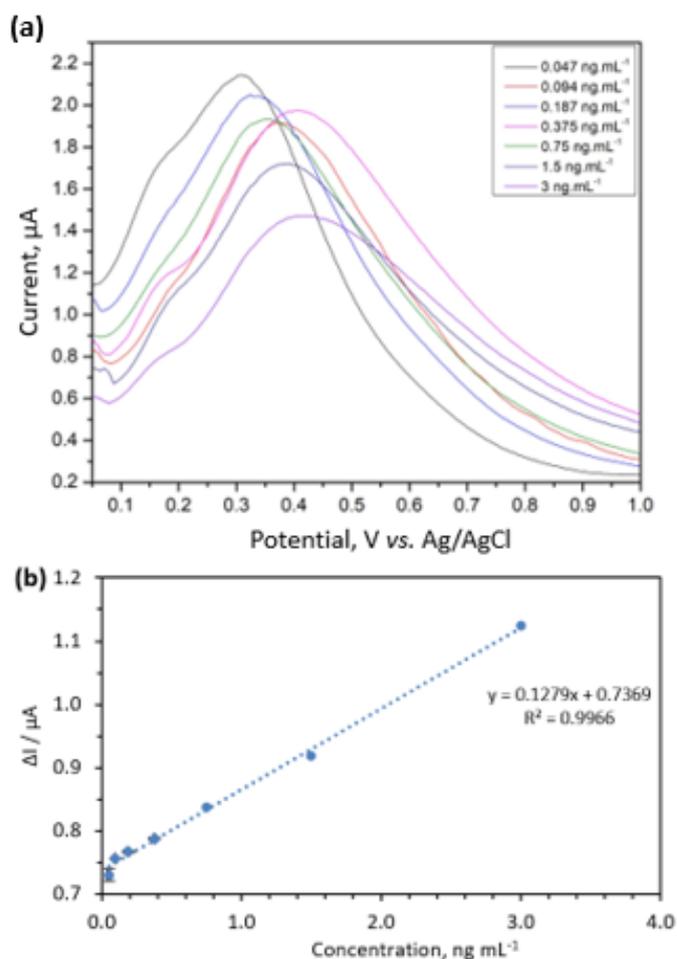
Figure 7. *DPVs of (a) aptasensor for ENaC concentration variation a → g (0.047, 0.094, 0.187, 0.375, 0.75, 1.5, 3) ng mL^{-1} and (b) aptasensor ENaC calibration curve*

The calibration curve in Figure 7b shows the optimum experimental conditions to determine the detection limit of the aptasensor. The linear regression equation obtained was $y = 0.1279x + 0.7369$, with R^2 of 0.9966. Based on the equation, y indicates the change in peak current and x for the analyte concentration. Determination of LOD and LOQ values in this work includes determining the smallest concentration of analyte that can be reliably measured by an analytical

procedure and will be used in real applications. The real application of this research is to detect analytes in a wide concentration range, so it is important to know the values of LOD and LOQ concentrations [51]. The detection and quantification limits [52] were determined as 0.113 and 0.343 ng mL^{-1}, respectively, with a precision of 98.320 %, accuracy of 99.485 % and recovery of 99.314 % at 0.75 ng mL^{-1} ENaC.

Aptasensor performance

The determination of the recovery test was carried out to validate the standard addition method, with the addition of the standard to the sample for determining the concentration of non-hypertensive individual samples. Spiking 0, 1, 2, and 3 ng mL^{-1} to the urine sample, and a standard addition curve was obtained as a voltammetric response by a linear regression equation. Previous research using the ELISA method showed that a patient of non-hypertensive, hypertensive with, and without a family history of hypertension, showed ENaC protein levels of 1.12, 2.7 and 4.0 ng mL^{-1}, respectively [53]. In this study, the concentration of ENaC contained in the sample was 0.021 ng mL^{-1}, what is less than for the hypertensive range. This suggests that using an aptasensor based on SPCE/silica-ceria/STV/aptamer is a rapid and easy method to detect ENaC in urine samples. The determined protein concentration of ENaC of 0.021 ng mL^{-1}, indicates that the developed aptasensor can sensitively determine ENaC in urine samples, making this method to be an alternative method to the ELISA. Measurement of ENaC concentration and recoveries obtained are listed in Table 4. The obtained recovery values in the range of 90-110 % verified the precision of the new method.

Table 4. *The recovery of method*

Spike sample concentraton, ng ml^{-1}	Recovery, %
0.0909	99.00 ± 0.007
0.1818	99.00 ± 0.001
0.2727	99.66 ± 0.002

The performance of the aptasensor regarding the repeatability of the signal on the calibration curve was carried out by a repeat test technique. Signal repetition is precise under the repeated conditions carried out in this experiment, so that the replication data under the optimum parameter conditions resulted in RSD value of 0.003 (acceptable) [54]. The calibration curve in Figure 7b shows the value of R^2 = 0.9966 (acceptable)[55] and high signal stability with a narrow error bar.

The selectivity of the aptamer to other proteins has been shown to be very good based on our previous study which was tested in silico. In that study, the performance of the aptasensor is performed using disposable electrodes [56].

The LOD and LOQ of the developed aptasensor were determined as 0.113 and 0.343 ng mL^{-1}, respectively. Compared to previously reported aptasensor results (Table 5), it appears that previously developed aptasensor by electrodeposition of silica had a lower LOD [3]. However, the electrodeposition method requires a longer time than dropping of composite solution directly onto the electrode surface (direct assembly), and thus is faster for detection as a point of care and mass production. In addition, it is still possible to distinguish the level of ENaC in normal urine from those with hypertension because of sodium intake.

***Table 5.** Comparison of the developed aptasensor performance to previously reported aptasensors*

Nanomaterial	Technique	Target	LOD	LOQ	Ref.
MSNs-NH$_2$	Fluorescence aptamer-based assay	Zearalenone	0.012 ng/mL	-	[57]
AuNPs/Fe$_3$O$_4$@ SiO$_2$/DABCO	CV, EIS	Epirubicin	0.04 µM	-	[58]
SNPs	Accurate fluorescent sensing	Aflatoxin B1	8 pg/mL	26 pg/mL	[59]
MSF	CV, DPV, EIS	Streptomycin	0.33 fg/mL	-	[60]
Silica microspheres-Au NPs	SWV	C-reactive protein	0.0017 ng/mL	-	[61]
AuNPs/FSN-NH$_2$	EIS, DPV	Tryptophan	0.01 nM (EIS) 0.026 nM (DPV)	-	[62]
SNP	Fluorescence emission spectra	Kanamycin	612 pM	-	[63]
GSGHs	CV, DPV	D-vasopressin (D-VP)	5 ng/mL	-	[64]
FcSH/SiNCs	DPV	Thrombin	0.06 nmol/L	-	[65]
GAuNPs composite	DPV	Norovirus	100 pM	-	[66]
SWCNTs	CV, DPV	Mycotoxin Ochrotoxin A	134 pM (serum) 58 pM (sample)	-	[67]
mSiO$_2$@ MWCNT nanocomposites	CV, DPV	Thrombin	50 fM	-	[68]
Ceria	DPV, EIS	ENaC protein	0.012 ng/mL	0.038 ng/mL	[3]
Silica-ceria nanocomposites	DPV	ENaC Protein	0.113 ng/mL	0.343 ng/mL	This work

Conclusions

SPCE-modified by natural silica-ceria composite exhibited a better ferro-ferricyanide current response than SPCE without modification. The [Fe(CN)$_6$]$^{3-/4-}$redox peak current showed an increase from 3.190 µA for bare SPCE to 9.073 µA for modified SPCE. This proves that the nanocomposite-modified SPCE electrode exhibits enhanced electron transfer which is generally beneficial for the detection process. The aptasensor method produces a quick diagnosis (point of care) when compared to existing methods such as ELISA method. The advantages of silica from natural materials could contribute to future development of aptasensors and increase their use value. In this work, the electrodes modified by natural silica-ceria nanocomposite have proven to detect ENaC protein as a biomarker of hypertension. The obtained LOD of 0.113 ng ml^{-1} suggests that this natural silica-based aptasensor can distinguish ENaC protein levels in urine samples of normal people and patients with non-hypertensive, hypertensive with, and without a family history of hypertension, which are higher*, i.e.* between 1.12 and 4.0 ng mL^{-1}.

References

[1]   X. Luo, A. Morrin, A. J. Killard, M. R. Smyth, Application of nanoparticles in electrochemical sensors and biosensors, *Electroanalysis* **18** (2006) 319-326. https://doi.org/10.1002/elan.200503415

[2]   C. E. Chivers, A. L. Koner, E. D. Lowe, M. Howarth, How the biotin-streptavidin interaction was made even stronger: Investigation via crystallography and a chimaeric tetramer, *Biochemical Journal* **435** (2011) 55-63. https://doi.org/10.1042/BJ20101593

[3]   Y. W. Hartati, D. R. Komala, D. Hendrati, S. Gaffar, A. Hardianto, Y. Sofiatin, H. H. Bahti, An aptasensor using ceria electrodeposited-screen-printed carbon electrode for detection of epithelial sodium channel protein as a hypertension biomarker, *Royal Society Open Science,* **8** (2021) 202040. https://doi.org/10.1098/rsos.202040

[4]   Y. W. Hartati, S. Gaffar, D. Alfiani, U. Pratomo, Y. Sofiatin, T. Subroto, A voltammetric immunosensor based on gold nanoparticle - Anti-ENaC bioconjugate for the detection of epithelial sodium channel (ENaC) protein as a biomarker of hypertension, *Sensing and Bio-Sensing Research* **29** (2020) 100343. https://doi.org/10.1016/j.sbsr.2020.100343

[5]   S. Ismail, N. A. Yusof, J. Abdullah, S. F. Abd Rahman, Development of Electrochemical Sensor Based on Silica/Gold Nanoparticles Modified Electrode for Detection of Arsenite, *IEEE Sensors Journal* **20** (2020) 3406-3414. https://doi.org/10.1109/JSEN.2019.2953799

[6]   S. Cajigas, D. Alzate, J. Orozco, Gold nanoparticle/DNA-based nanobioconjugate for electrochemical detection of Zika virus, *Microchimica Acta* **187** (2020) 594. https://doi.org/10.1007/s00604-020-04568-1

[7]   C. Núñez, J. J. Triviño, V. Arancibia, A electrochemical biosensor for As(III) detection based on the catalytic activity of Alcaligenes faecalis immobilized on a gold nanoparticle–modified screen–printed carbon electrode, *Talanta* **223** (2021) 121702. https://doi.org/10.1016/j.talanta.2020.121702

[8]   A. K. Sari, Y. W. Hartati, S. Gaffar, I. Anshori, D. Hidayat, H. L. Wiraswati, The optimization of an electrochemical aptasensor to detect RBD protein S SARS-CoV-2 as a biomarker of COVID-19 using screen-printed carbon electrode/AuNP, *Journal of Electrochemical Science and Engineering.* **12** (2022) 219–235 https://doi.org/10.5599/jese.1206

[9]   R. Sakthivel, M. Annalakshmi, S.M. Chen, S. Kubendhiran, R. Anbazhagan, H. C. Tsai, A novel sensitive and reliable electrochemical determination of palmatine based on CeO_2/RGO/MWCNT ternary composite, , *Journal of the Taiwan Institute of Chemical Engineers* **96** (2019) 549-558. https://doi.org/10.1016/j.jtice.2018.11.008

[10] R. C. de Carvalho, A. J. Betts, J. F. Cassidy, Diclofenac determination using CeO_2 nanoparticle modified screen-printed electrodes – A study of background correction, *Microchemical Journal* **158** (2020) 105258. https://doi.org/10.1016/j.microc.2020.105258

[11] Y. Bai, H. Yang, W. Yang, Y. Li, C. Sun, Gold nanoparticles-mesoporous silica composite used as an enzyme immobilization matrix for amperometric glucose biosensor construction, *Sensors and Actuators B: Chemical* **124** (2007) 179-186. https://doi.org/10.1016/j.snb.2006.12.020

[12] L. Zhao, Y. Huang, Y. Dong, X. Han, S. Wang, X. Liang, Aptamers and aptasensors for highly specific recognition and sensitive detection of marine biotoxins: Recent advances and perspectives, *Toxins* **10** (2018) 427. https://doi.org/10.3390/toxins10110427

[13] J. Fei, W. Dou, G. Zhao, A sandwich electrochemical immunoassay for Salmonella pullorum and Salmonella gallinarum based on a $AuNPs/SiO_2/Fe_3O_4$ adsorbing antibody and 4 channel screen printed carbon electrode electrodeposited gold nanoparticles, *RSC Advances* **5** (2015) 74548-74556. https://doi.org/10.1039/c5ra12491c

[14] A. Kornii, V. Saska, V. V. Lisnyak, O. Tananaiko, Carbon Nanostructured Screen-printed Electrodes Modified with $CuO/Glucose Oxidase/Maltase/SiO_2$ Composite Film for Maltose Determination, *Electroanalysis* **32** (2020) 1468-1479.

https://doi.org/10.1002/elan.202000059

[15]   J. P. Metters, R. O. Kadara, C. E. Banks, New directions in screen printed electroanalytical sensors: An overview of recent developments, *Analyst* **136** (2011) 1067-1076. https://doi.org/10.1039/c0an00894j

[16]   S. H. Wu, H. P. Lin, Synthesis of mesoporous silica nanoparticles, *Chemical Society Reviews* **42** (2013) 3862-3875. https://doi.org/10.1039/c3cs35405a

[17]   Y. Sun, Y. Lin, C. Ding, W. Sun, Y. Dai, X. Zhu, H. Liu, C. Luo, An ultrasensitive and ultraselective chemiluminescence aptasensor for dopamine detection based on aptamers modified magnetic mesoporous silica @ graphite oxide polymers, *Sensors and Actuators B: Chemical* **257** (2018) 312-323. https://doi.org/10.1016/j.snb.2017.10.171

[18]   A. Walcarius, Silica-based electrochemical sensors and biosensors: Recent trends, *Current Opinion in Electrochemistry* **10** (2018) 88-97. https://doi.org/10.1016/j.coelec.2018.03.017

[19]   J. Li, Y. Hao, H. Li, M. Xia, X. Sun, L. Wang, Direct synthesis of CeO_2/SiO_2 mesostructured composite materials via sol-gel process, *Microporous and Mesoporous Materials* **120** (2009) 421-425. https://doi.org/10.1016/j.micromeso.2008.12.014

[20]   M. L. Firdaus, F. E. Madina, Y. F. Sasti, R. Elvia, S. N. Ishmah, D. R. Eddy, A. P. Cid-Andres, Silica extraction from beach sand for dyes removal: Isotherms, kinetics and thermodynamics, *Rasayan Journal of Chemistry* **13** (2020) 249-254. https://doi.org/10.31788/RJC.2020.1315496

[21]   S. Ismail, N. A. Yusof, J. Abdullah, S. F. Abd Rahman, Electrochemical detection of arsenite using a silica nanoparticles-modified screen-printed carbon electrode, *Materials* **13** (2020) 3168. https://doi.org/10.3390/ma13143168

[22]   A. Sánchez, S. Morante-Zarcero, D. Pérez-Quintanilla, I. Sierra, I. Del Hierro, Development of screen-printed carbon electrodes modified with functionalized mesoporous silica nanoparticles: Application to voltammetric stripping determination of Pb(II) in non-pretreated natural waters, *Electrochimica Acta* **55** (2010) 6983-6990. https://doi.org/10.1016/j.electacta.2010.06.090

[23]   W. Siangproh, W. Dungchai, P. Rattanarat, O. Chailapakul, Nanoparticle-based electrochemical detection in conventional and miniaturized systems and their bioanalytical applications: A review, *Analytica Chimica Acta* **690** (2011) 10-25. https://doi.org/10.1016/j.aca.2011.01.054

[24]   S. Xunwen, Z. Liqun, L. Weiping, L. Huicong, Y. Hui, The synthesis of monodispersed M-CeO_2/SiO_2 nanoparticles and formation of UV absorption coatings with them, *Royal Society of Chemistry* **10** (2020) 4554-4560. https://doi.org/10.1039/c9ra08975f

[25]   Q. Ma, Y. Li, X. Su, Silica-nanobead-based sensors for analytical and bioanalytical applications, *Trends in Analytical Chemistry* **74** (2015) 130-145. https://doi.org/10.1016/j.trac.2015.06.006

[26]   S. Damiati, C. Haslam, S. Sopstad, M. Peacock, T. Whitley, P. Davey, S. A. Awan, Sensitivity Comparison of Macro-and Micro-Electrochemical Biosensors for Human Chorionic Gonadotropin (hCG) Biomarker Detection, *IEEE Access* **7** (2019) 94048-94058. https://doi.org/10.1109/ACCESS.2019.2928132

[27]   Y. W. Hartati, S. F. Yusup, Fitrilawati, S. Wyantuti, Y. Sofiatin, S. Gaffar, A voltammetric epithelial sodium channels immunosensor using screen-printed carbon electrode modified with reduced graphene oxide, *Current Chemistry Letters* **9** (2020) 151-160. https://doi.org/10.5267/j.ccl.2020.2.001

[28]   S. Oparil, M. C. Acelajado, G. L. Bakris, D. R. Berlowitz, R. Cífková, A. F. Dominiczak, G. Grassi, J. Jordan, N. R. Poulter, A. Rodgers, P. K. Whelton, Hypertension, *Nature Reviews Disease Primers* **4** (2018) 18014. https://doi.org/10.1038/nrdp.2018.14

[29]   H. W. Choi, K. H. Lee, N. H. Hur, H. B. Lim, Cerium oxide-deposited mesoporous silica nanoparticles for the determination of carcinoembryonic antigen in serum using inductively coupled plasma-mass spectrometry, *Analytica Chimica Acta* **847** (2014) 10-15. https://doi.org/10.1016/j.aca.2014.08.041

[30]   G. Frindt, D. Gravotta, L. G. Palmer, Regulation of ENaC trafficking in rat kidney, *Journal of General Physiology* **147** (2016) 217-227. https://doi.org/10.1085/jgp.201511533

[31]   E. Reus-Chavarría, I. Martínez-Vieyra, C. Salinas-Nolasco, A. E. Chávez-Piña, J. V. Méndez-Méndez, E. O. López-Villegas, A. Sosa-Peinado, D. Cerecedo, Enhanced expression of the Epithelial Sodium Channel in neutrophils from hypertensive patients, *Biochimica Biophysica Acta - Biomembranes* **1861** (2019) 387-402. https://doi.org/10.1016/j.bbamem.2018.11.003

[32]   Rajesh, S. Singal, R. K. Kotnala, Single Frequency Impedance Analysis on Reduced Graphene Oxide Screen-Printed Electrode for Biomolecular Detection, *Applied Biochemistry and Biotechnology* **183** (2017) 672-683. https://doi.org/10.1007/s12010-017-2510-8

[33]   Y. W. Hartati, S. Gaffar, D. Alfiani, U. Pratomo, Y. Sofiatin, T. Subroto, A voltammetric immunosensor based on gold nanoparticle - Anti-ENaC bioconjugate for the detection of epithelial sodium channel (ENaC) protein as a biomarker of hypertension, *Sensing and Bio-Sensing Research* **29** (2020) 100343. https://doi.org/10.1016/j.sbsr.2020.100343

[34]   B. Kayhan, N. Kayabas, Aptamers: An in vitro Evolution of Therapeutic and Diagnostic Applications in Medicine, *Disease and Molecular Medicine* **1** (2013) 54-60. https://doi.org/10.5455/dmm.20131104040658

[35]   P. Yáñez-Sedeño, J. M. Pingarrón, Gold nanoparticle-based electrochemical biosensors, *Analytical and Bioanalytical Chemistry* **382** (2005) 884-886. https://doi.org/10.1007/s00216-005-3221-5

[36]   C. M. Dundas, D. Demonte, S. Park, Streptavidin-biotin technology: Improvements and innovations in chemical and biological applications, *Applied Microbiology and Biotechnology.* **97** (2013) 9343-9353. https://doi.org/10.1007/s00253-013-5232-z

[37]   D. R. Komala, A. Hardianto, S. Gaffar, Y. W. Hartati, An epithelial sodium channel (ENaC)-specific aptamer determined through structure-based virtual screening for the development of hypertension early detection system, *Pharmaceutical Sciences* **27** (2021) 67-75. https://doi.org/10.34172/PS.2020.63

[38]   M. M. Ali, H. S. Mahdi, A. Parveen, A. Azam, Optical properties of cerium oxide (CeO_2) nanoparticles synthesized by hydroxide mediated method, *AIP Conference Proceedings* **1953** (2018) 030044. https://doi.org/10.1063/1.5032379

[39]   S. N. Ishmah, M. D. Permana, M. L. Firdaus, D. R. Eddy, Extraction of Silica from Bengkulu Beach Sand using Alkali Fusion Method, *PENDIPA Journal of Science Education* **4** (2020) 1-5. https://doi.org/10.33369/pendipa.4.2.1-5

[40]   S. Phanichphant, A. Nakaruk, D. Channei, Photocatalytic activity of the binary composite CeO2/SiO2 for degradation of dye, *Applied Surface Science* **387** (2016) 214-220. https://doi.org/10.1016/j.apsusc.2016.06.072

[41]   M. L. Yola, N. Atar, A novel detection approach for serotonin by graphene quantum dots/two-dimensional (2D) hexagonal boron nitride nanosheets with molecularly imprinted polymer, *Applied Surface Science* **458** (2018) 648-655. https://doi.org/10.1016/j.apsusc.2018.07.142

[42]   R. Sha, N. Vishnu, S. Badhulika, MoS2 based ultra-low-cost, flexible, non-enzymatic and non-invasive electrochemical sensor for highly selective detection of Uric acid in human urine samples, *Sensors and Actuators B: Chemical* **279** (2019) 53-60.

https://doi.org/10.1016/j.snb.2018.09.106

[43] M. S. Pujar, S.M. Hunagund, V. R. Desai, S. Patil, A. H. Sidarai, One-step synthesis and characterizations of cerium oxide nanoparticles in an ambient temperature via Co-precipitation method, *AIP Conference Proceedings* **1942** (2018) 050026. https://doi.org/10.1063/1.5028657

[44] J. Calvache-Muñoz, F.A. Prado, J. E. Rodríguez-Páez, Cerium oxide nanoparticles: Synthesis, characterization and tentative mechanism of particle formation, *Colloids and Surfaces A: Physicochemical and Engineering Aspects* **529** (2017) 146–159. https://doi.org/10.1016/j.colsurfa.2017.05.059

[45] R. Dalmis, I. Birlik, N.F. Ak Azem, E. Celik, Structurally colored silica photonic crystal coatings modified by Ce or Eu rare-earth dopants, *Colloids and Surfaces A: Physicochemical and Engineering Aspects* **603** (2020) 125138. https://doi.org/10.1016/j.colsurfa.2020.125138

[46] F. Vaja Dumitru, O. Oprea, D. Ficai, A. Ficai, C. Guran, Synthesis of CeO_2 nanoparticles on the mesoporous silica support via nanocasting, *Digest Journal of Nanomaterials and Biostructures* **9** (2014) 187-195.

[47] D. K. Maharani, R. Hidayah, Preparation And Characterization Of Chitosan-ZnO/Al_2O_3 Composite, *Molekul* **10** (2015) 9-18. http://dx.doi.org/10.20884/1.jm.2015.10.1.167

[48] S. K. Kannan, M. Sundrarajan, A green approach for the synthesis of a cerium oxide nanoparticle: Characterization and antibacterial activity, *International Journal of Nanoscience.* **13** (2014) 1450018. https://doi.org/10.1142/S0219581X14500185

[49] J. E. ten Elshof, *Chemical solution deposition techniques for epitaxial growth of complex oxides*, in *Epitaxial Growth of Complex Metal Oxides*, G. Koster, M. Huijben, G. Rijnders (Eds.), Woodhead Publishing, Enschede, Netherlands, 2015. https://doi.org/10.1016/B978-1-78242-245-7.00004-X

[50] D. E. Hyre, Cooperative hydrogen bond interactions in the streptavidin-biotin system, *Protein Science* **15** (2006) 459-467. https://doi.org/10.1110/ps.051970306

[51] D. A. Armbruster, T. Pry, Limit of blank, limit of detection and limit of quantitation, The *Clinical Biochemist Reviews* **29** (2008) S49-S52. PMID: 18852857

[52] J. C. Miller, J. N. Miller, *Statistika untuk kimia analitik*, ITB Press, 1991. ISBN 9798001486

[53] Y. Sofiatin, R. MA Roesli, Detection of Urinary Epithelial Sodium Channel (ENaC) Protein, *American Journal of Clinical Medicine Research* **6** (2018) 20-23. https://doi.org/10.12691/ajcmr-6-2-1

[54] AOAC International, Appendix F: Guidelines for Standard Method Performance Requirements, *Journal of AOAC International and Official Method of Analysis* **9** (2016) 1-18.

[55] C. B. L. Jumbe, Cointegration and causality between electricity consumption and GDP: Empirical evidence from Malawi, *Energy Economics* **26** (2004) 61-68. https://doi.org/10.1016/S0140-9883(03)00058-6

[56] H. A. Samie, M. Arvand, Label-free electrochemical aptasensor for progesterone detection in biological fluids, *Bioelectrochemistry* **133** (2020) 107489. https://doi.org/10.1016/j.bioelechem.2020.107489

[57] H. Tan, T. Guo, H. Zhou, H. Dai, Y. Yu, H. Zhu, H. Wang, Y. Fu, Y. Zhang, L. Ma, A simple mesoporous silica nanoparticle-based fluorescence aptasensor for the detection of zearalenone in grain and cereal products, *Analytical and Bioanalytical Chemistry* **412** (2020) 5627-5635. https://doi.org/10.1007/s00216-020-02778-3

[58] A. B. Hashkavayi, J. B. Raoof, Design an aptasensor based on structure-switching aptamer on dendritic gold nanostructures/Fe_3O_4@SiO_2/DABCO modified screen printed

electrode for highly selective detection of epirubicin, *Biosensors and Bioelectronics* **91** (2017) 650-657. https://doi.org/10.1016/j.bios.2017.01.025

[59]　S. M. Taghdisi, N. M. Danesh, M. Ramezani, K. Abnous, A new amplified fluorescent aptasensor based on hairpin structure of G-quadruplex oligonucleotide-Aptamer chimera and silica nanoparticles for sensitive detection of aflatoxin B 1 in the grape juice, *Food Chemistry* **268** (2018) 342-346. https://doi.org/10.1016/j.foodchem.2018.06.101

[60]　M. Roushani, K. Ghanbari, An electrochemical aptasensor for streptomycin based on covalent attachment of the aptamer onto a mesoporous silica thin film-coated gold electrode, *Microchimica Acta* **186** (2019) 115. https://doi.org/10.1007/s00604-018-3191-x

[61]　J. Wang, J. Guo, J. Zhang, W. Zhang, Y. Zhang, RNA aptamer-based electrochemical aptasensor for C-reactive protein detection using functionalized silica microspheres as immunoprobes, *Biosensors and Bioelectronics* **95** (2017) 100-105. https://doi.org/10.1016/j.bios.2017.04.014

[62]　A. B. Hashkavayi, J. B. Raoof, R. Ojani, Construction of a highly sensitive signal-on aptasensor based on gold nanoparticles/functionalized silica nanoparticles for selective detection of tryptophan, *Analytical and Bioanalytical Chemistry* **409** (2017) 6429-6438. https://doi.org/10.1007/s00216-017-0588-z

[63]　L. S. Khabbaz, M. Hassanzadeh-Khayyat, P. Zaree, M. Ramezani, K. Abnous, S. M. Taghdisi, Detection of kanamycin by using an aptamer-based biosensor using silica nanoparticles, *Analytical Methods* **7** (2015) 8611-8616. https://doi.org/10.1039/c5ay01807b

[64]　Y. Du, S. Guo, H. Qin, S. Dong, E. Wang, Target-induced conjunction of split aptamer as new chiral selector for oligopeptide on graphene–mesoporous silica–gold nanoparticle hybrids modified sensing platform, *Chemical Communications* **48** (2012) 799-801. https://doi.org/10.1039/c1cc15303j

[65]　Y. Wang, X. He, K. Wang, X. Ni, J. Su, Z. Chen, Electrochemical detection of thrombin based on aptamer and ferrocenylhexanethiol loaded silica nanocapsules, *Biosensors and Bioelectronics* **26** (2011) 3536-3541. https://doi.org/10.1016/j.bios.2011.01.041

[66]　R. Chand, S. Neethirajan, Microfluidic platform integrated with graphene-gold nano-composite aptasensor for one-step detection of norovirus, *Biosensors and Bioelectronics* **98** (2017) 47-53. https://doi.org/10.1016/j.bios.2017.06.026

[67]　K. Abnous, N. M. Danesh, M. Alibolandi, M. Ramezani, S. M. Taghdisi, Amperometric aptasensor for ochratoxin A based on the use of a gold electrode modified with aptamer, complementary DNA, SWCNTs and the redox marker Methylene Blue, *Microchimica Acta* **184** (2017) 1151-1159. https://doi.org/10.1007/s00604-017-2113-7

[68]　J. Zhang, Y. Chai, R. Yuan, Y. Yuan, L. Bai, S. Xie, A highly sensitive electrochemical aptasensor for thrombin detection using functionalized mesoporous silica@multiwalled carbon nanotubes as signal tags and DNAzyme signal amplification, *Analyst* **138** (2013) 6938-6945. https://doi.org/10.1039/c3an01587d